Magnetization reversal in exchange biased IrMn/Fe ring arrays

Yu-feng Hou, Qing-feng Zhan, and Kannan M. Krishnan[a)]
Department of Materials Science, University of Washington, Seattle, Washington 98195, USA

(Received 8 November 2010; accepted 6 January 2011; published online 28 January 2011)

We investigated the effect of exchange bias on the magnetization reversal behavior in ring-shaped IrMn/Fe lithographic structures. The magnetic anisotropy geometry of the exchange biased ring is revealed by fitting for the angular dependence of the exchange bias, H_{eb}, and coercivity, H_c. Magnetic force microscopy images obtained at different field values along the hysteresis loop show that along the bias direction, the ring exhibits a magnetic reversal via nonuniform domain nucleation while perpendicular to the bias direction, the magnetic reversal occurs via coherent rotation. The difference in magnetic switching modes for these two field orientations is confirmed by micromagnetic simulations and interpreted by the effective field model. © *2011 American Institute of Physics*. [doi:10.1063/1.3549187]

With the advancement in fabrication techniques to miniaturize the physical dimensions of magnetic elements,[1] there has been a considerable interest in lithographically defined structures from both application and scientific points of view.[2] When the dimensions of the patterned magnets become comparable to the ferromagnetic domain wall width, their properties significantly differ from their bulk counterparts.[3] In this regard, lithographically defined magnetic thin film rings have become the focus of intensive research in the past few years because of their distinct magnetic states[4] and highly reproducible switching behavior, which makes them potential candidates for the magnetoelectronic[5] and magnetic sensing devices.[6] In order to control the magnetic states and the switching process of ring structures, many variations have been made to the ring shapes, for example, by introducing notches or flat edges to the ring,[7] decentering the ring,[8] or even altering the shape of the rings into triangles or squares.[9,10] The effect of magnetocrystalline anisotropy on the rings has also been studied in epitaxial ring structures.[11] Alternately, exchange bias (EB), which refers to the shift of the hysteresis loop in the magnetic field direction, can also serve as a tunable source of unidirectional anisotropy to tailor the magnetic properties of rings. So far, very little effort has been devoted to the study of such exchange biased rings.[12–14] EB induced asymmetric magnetization behavior along the bias direction has been observed in magnetic ring structures,[15] but the detailed mechanism of magnetic reversal is not well understood. Here, magnetization reversal mechanism of micron-size EB IrMn/Fe rings is studied using angular dependent magneto-optical Kerr effect (MOKE) magnetometry, magnetic force microscopy (MFM), and micromagnetic simulations. The results are also compared with the unbiased Fe rings. Drastically different magnetic reversal mechanisms are observed in the exchange biased rings when the field is applied either along or perpendicular to the bias direction. Micromagnetic simulations are performed to reveal the spin configurations of the EB rings during the reversal process for these two field orientations.

Arrays of circular Ta (1 nm)/Cu (5 nm)/IrMn (10 nm)/Fe (10 nm)/Ta (3 nm) multilayer rings with outer and inner diameters $d_{out}/d_{in}=2.5\ \mu m/0.8\ \mu m$ and inter-ring distance 3 μm, as schematically displayed in Fig. 1(a), were fabricated on Si/SiO_2 substrates via a mask-transferred lithographic process, described elsewhere in detail.[16] The two bottom layers, Ta (1 nm)/Cu (5 nm), serve as seeding layers to induce the (111) texture growth of IrMn.[17] A 3 nm thick Ta capping layer was deposited on the top to protect the whole structure from oxidation. Figure 1(b) shows scanning electron microscope images of the multilayer ring arrays and a detailed view of a single ring. In order to introduce an EB, the as-prepared sample was heated to 600 K in vacuum and then cooled to room temperature under an external field of 200 Oe applied in the surface plane of the sample. To facilitate the understanding of the effect of EB, another reference sample without the antiferromagnetic layer, i.e., Ta (1 nm)/Cu (5 nm)/Fe (10 nm)/Ta (3 nm), was also prepared in the same process.

M-H hysteresis loops of both exchange biased and unbiased ring samples were subsequently measured at room temperature with an in-plane applied magnetic field, using a longitudinal MOKE setup. To improve the signal-to-noise ratio, each loop was obtained by averaging the measured results over 20 times. The hysteresis loop of the unbiased Fe rings is shown in Fig. 2(a). The red and the blue curves represent the descending and the ascending branches of the loop, respectively. No significant differences in the shape of the hysteresis loop were observed when measuring along different directions of the sample, indicating that the intrinsic magnetocrystalline anisotropy of Fe and the dipolar interactions among rings were negligible. The experimentally measured

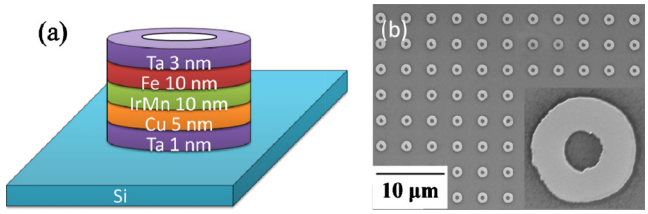

FIG. 1. (Color online) (a) Schematic structure of multilayer ring arrays. (b) Scanning electron microscopic images of the sample. A detailed image of one ring is shown on the bottom right corner.

a)Author to whom correspondence should be addressed. Electronic mail: kannanmk@uw.edu.

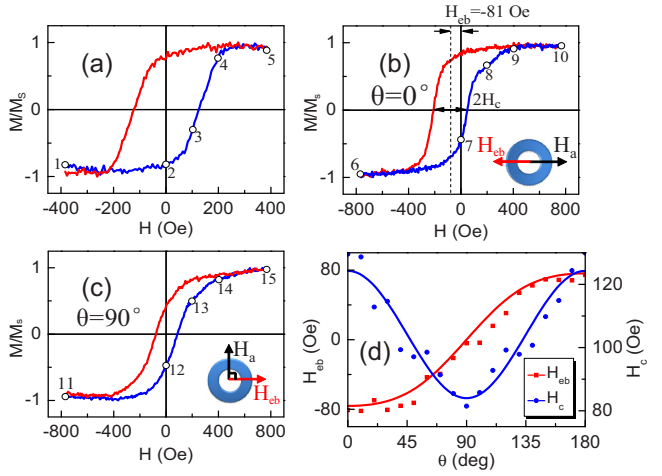

FIG. 2. (Color online) M-H hysteresis loops of (a) the unbiased Fe ring arrays, and the exchange biased ring arrays with the field applied (b) along and (c) perpendicular to the bias direction. (d) The EB H_{eb} and the coercivity H_c of exchange biased rings as a function of the field orientation θ.

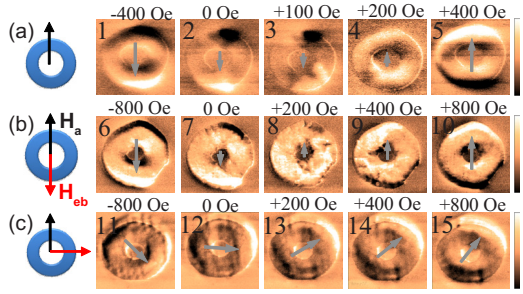

FIG. 3. (Color online) Selected MFM images showing the magnetic reversal process for (a) the unbiased Fe rings at marked field values. Magnitude and direction of the magnetization is marked by the gray arrows on the ring. For the exchange biased rings (b) along the field cool direction at marked field values. (c) Perpendicular to the bias direction. The corresponding magnetic field values are the same as in (b). However, the images show that the EB ensures that there is always a significant component of the magnetization along H_{eb}.

coercivity of the unbiased ring is 124 Oe. For exchange biased rings, the hysteresis behavior was measured with the magnetic field applied at different angles, θ, with respect to the bias direction. Figures 2(b) and 2(c) are the hysteresis loops of IrMn/Fe exchange biased rings measured along $\theta=0°$ and 90°, respectively. When the field is applied along the bias direction (i.e., $\theta=0°$), the hysteresis loop possesses a similar shape as that of the unbiased Fe rings, with a slightly higher coercive field ($H_c=130$ Oe) and a shift ($H_{eb}=-81$ Oe) of the loop in the negative field direction due to the interfacial exchange coupling between Fe and IrMn layers. The hysteresis loop measured perpendicularly to the bias direction (i.e., $\theta=90°$) exhibits a coercivity of 81 Oe but no EB. This indicates that during the field cooling procedure, the interfacial uncompensated spins of the antiferromagnetic layer were effectively aligned in the field direction, thus exerting a unidirectional anisotropy on the ferromagnetic layer due to the interfacial exchange coupling. The angular dependence of both the EB $H_{eb}(\theta)$ and the coercivity $H_c(\theta)$ on this field orientation, θ is studied via a series of measurements varying θ from 0° to 180° in steps of 10°. The values of $H_{eb}(\theta)$ and $H_c(\theta)$ are obtained at each θ value and the results are shown in Fig. 2(d). $H_{eb}(\theta)$ shows a unidirectional symmetry about the bias direction, i.e., $H_{eb}(\pi+\theta)=-H_{eb}(\theta)$. However, $H_c(\theta)$ exhibits a twofold uniaxial symmetry about the bias axis, i.e., $H_c(\pi+\theta)=H_c(\theta)$. Considering the symmetry of the magnetic anisotropy energy,[18] the value of $H_{eb}(\theta)$ and $H_c(\theta)$ can be described by Fourier cosine series with odd and even terms, respectively. That is, $H_{eb}(\theta)=H_{eb}(0)\Sigma_{n=odd}b_n\cos(n\theta)$ and $H_c(\theta)=H_c(0)\Sigma_{n=even}b_n\cos(n\theta)$. For our samples, the numerical fitting results show the EB follows the simple cosine relation: $H_{eb}(\theta)=-81\ \text{Oe}\cos(\theta)$, which results directly from the unidirectional anisotropy caused by EB, and the coercivity follows the relation: $H_c=104\ \text{Oe}\ [1+0.2\cos(2\theta)]$, which indicates that the EB induces a collinear uniaxial anisotropy as well.

The magnetic domain configurations of the samples were investigated by MFM with magnetic field applied parallel to the sample surface, using 45 nm CoPt/FePt coated high coercivity probes with a lift height of 30 nm. Figures 3(a)–3(c) shows selected MFM images measured at the nominal values of magnetic fields as marked in Figs. 2(a)–2(c). Since no significant asymmetry in the magnetization reversal is observed with increasing or decreasing field, we only display the images at different points of the ascending branch. Figure 3(a) shows the MFM images for the unbiased Fe rings varied from the negative to positive saturation, corresponding to the ascending branch in Fig. 2(a). For Fig. 3(a) (1), the applied field is −400 Oe and the ring is negatively saturated. A black and a white area with dipolar contrast are observed at the edge of the ring along the field direction, indicating the formation of magnetic poles in a saturated single domain state. In Fig. 3(a), (2) (3), (4), and (5) correspond to the applied field value of 0, 100, 200, and 400 Oe, respectively. As the field increases, the areas of the dipolar contrast gradually shrink in size, which indicates the elimination of the ferromagnetic domain in the negative field direction and the creation of the domain aligned along the positive direction, until the field reverses its direction to positive. After the field exceeds the coercivity and reaches 200 Oe, the dipolar contrast on the ring is suddenly reversed in the direction with much weaker strength [Fig. 3(a) (4)]. Upon further increasing of the field in the positive direction, the reversed dipolar contrast is strengthened and saturated at 400 Oe [Fig. 3(a) (5)]. The series of images in Fig. 3(a) indicates that the magnetization reversal of the unbiased ring is dominated by the nonuniform domain nucleation. Figure 3(b) illustrates the magnetic reversal process of the exchange biased ring when the field is applied along the bias direction, which corresponds to the ascending branch of the hysteresis loop in Fig. 2(b). In Fig. 3(b) (6)–(10), the applied field is varied from −800 to 800 Oe. Similar to the unbiased ring, the dipolar contrast observed at negative saturation [Fig. 3(b) (6)] fades progressively as the field approaches the coercivity, and abruptly switches its direction at positive 400 Oe [Fig. 3(b) (8)], and gets enhanced and positively saturated at 800 Oe [Fig. 3(b) (10)]. The MFM results indicate the magnetic reversal mechanism in the exchange biased ring for the field applied along the field cool direction remains the same as the unbiased Fe ring. However, Fig. 3(c) reveals that the magnetic reversal mode, when the applied field is perpendicular to the bias direction (i.e., $\theta=90°$) is drastically different. As the field is increased from the negative saturation and then reversed the magnetization direction as depicted by the axis of the dipolar contrast slowly rotates to the bias direc-

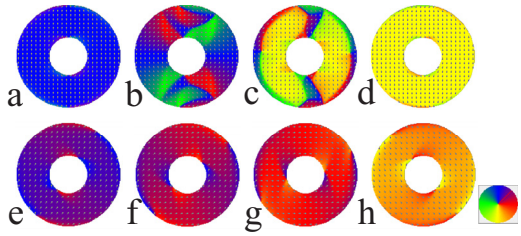

FIG. 4. (Color online) Micromagnetic simulated spin configurations of the exchange biased ring in the magnetic reversal process [(a)–(d)] along the bias direction, and [(e)–(h)] perpendicular to the bias direction. The magnetization direction is indicated by the color wheel or overlaid arrows.

tion, and then to the positive saturation, as shown in Fig. 3(c) (11)–(15). The rotation of the dipolar contrast implies that the magnetization of the rings roughly remains in its single domain state but rotates from the negative to the positive saturation with increasing field. That is to say, the magnetic reversal mechanism for the exchange biased ring measured perpendicular to the bias direction is dominated by coherent rotation, which is significantly different from the measurement along the EB.

Micromagnetic simulations of the magnetic reversal process of exchange biased rings have also been performed both along the bias direction ($\theta=0°$) and perpendicular to the bias direction ($\theta=90°$), using the LLG micromagnetic simulator.[19] The saturation magnetization and the exchange stiffness constant of the Fe layer are set at the value of bulk Fe: $M_s=1714$ emu/cm^3 and $A=12$ μerg/cm. The cubic magnetocrystalline anisotropy with randomly distributed easy axes is assigned to each of the $5\times5\times5$ nm^3 cells of Fe due to the polycrystalline structure of Fe ring layer. The EB field arising from the interface exchange coupling between IrMn and Fe layers is simulated as an additional static field of magnitude $H_{eb}=-81$ Oe, applied in the direction of $\theta=0°$. In Fig. 4, the first row shows the simulated magnetization reversal process for $\theta=0°$, while the second row shows the case for $\theta=90°$. The magnetization direction is indicated by the color wheel and the overlaid arrows. In Fig. 4(a), the ring is magnetically saturated in the negative field direction. As the field increases, magnetic domains along other directions start to nucleate, as shown by the red and green regions in Fig. 4(b). Finally, the magnetic domains of the positive direction expand over others [Fig. 4(c)], and reach the positive saturation in Fig. 4(d). The simulation results confirm the nucleation and growth observed in MFM imaging. When the external field is perpendicular to the bias direction, as the field increases from negative saturation, the ring remains in its single domain state with the dipole direction gradually rotating from the negative field direction [Fig. 4(e)] to the bias direction [Fig. 4(g)], and finally reaches the positive saturation [Fig. 4(h)].

The differences in magnetic reversal modes at different field orientation could be qualitatively explained by an effective field model developed by Beckmann *et al.*[20] This model considers three contributions to the effective field H_{eff} acting on the ferromagnetic layer during the process of magnetic reversal. They are the exchange field, H_{eb}, in the field-cool direction, the external magnetic field, H_a, and the uniaxial anisotropy field, H_u. In the case of $\theta=0°$, the EB field and the anisotropy field are collinear with the applied field, thus the effective field is aligned with the magnetization, which favors the domain nucleation mode for the magnetization reversal. In the case of $\theta=90°$, the external magnetic field, H_a, is perpendicular to the exchange field, H_{eb}, and the anisotropy field, H_u. Thus, the effective field has a large angle with respect to the magnetization, which lies in the easy direction given by H_{eb} and H_u, leading to a strong torque that favors the coherent rotation mode of magnetic reversal.

The authors would like to thank Wei Zhang and Dr. Dirk N. Weiss for the technical help on the photolithography and Dr. M. Sheinfein for help on micromagnetic simulations. This work was supported by DoE/BES under Grant No. ER45987.

[1] A. O. Adeyeye and N. Singh, J. Phys. D **41**, 153001 (2008).
[2] H. X. Wei, F. Q. Zhu, X. F. Han, Z. C. Wen, and C. L. Chien, Phys. Rev. B **77**, 224432 (2008).
[3] S. D. Bader, Rev. Mod. Phys. **78**, 1 (2006).
[4] M. Kläui, L. Lopez-Diaz, J. Rothman, C. A. F. Vaz, J. A. C. Bland, and Z. Cui, J. Magn. Magn. Mater. **240**, 7 (2002).
[5] J. G. Zhu, Y. Zheng, and G. A. Prinz, J. Appl. Phys. **87**, 6668 (2000).
[6] J. Llandro, T. J. Hayward, D. Morecroft, J. A. C. Bland, F. J. Castaño, I. A. Colin, and C. A. Ross, Appl. Phys. Lett. **91**, 203904 (2007).
[7] M. Kläui, C. A. F. Vaz, J. A. C. Bland, W. Wernsdorfer, G. Faini, and E. Cambril, Appl. Phys. Lett. **81**, 108 (2002).
[8] F. Q. Zhu, G. W. Chern, O. Tchernyshyov, X. C. Zhu, J. G. Zhu, and C. L. Chien, Phys. Rev. Lett. **96**, 027205 (2006).
[9] P. Vavassori, M. Grimsditch, V. Novosad, V. Metlushko, and B. Illic, Phys. Rev. B **67**, 134429 (2003).
[10] A. O. Adeyeye, S. Goolaup, N. Singh, C. C. Wang, X. S. Gao, C. A. Ross, W. Jung, and F. J. Castano, J. Phys. D **40**, 6479 (2007).
[11] C. A. F. Vaz, L. Lopez-Diaz, M. Klaui, J. A. C. Bland, T. L. Monchesky, J. Unguris, and Z. Cui, Phys. Rev. B **67**, 140405 (2003).
[12] Z. B. Guo, Y. K. Zheng, K. B. Li, Z. Y. Liu, P. Luo, and Y. H. Wu, J. Appl. Phys. **95**, 4918 (2004).
[13] W. Jung, F. J. Castano, and C. A. Ross, Phys. Rev. Lett. **97**, 247209 (2006).
[14] W. Jung, F. J. Castano, D. Morecroft, C. A. Ross, R. Menon, and H. I. Smith, J. Appl. Phys. **97**, 10K113 (2005).
[15] D. Tripathy, A. O. Adeyeye, N. Singh, and R. L. Stamps, Nanotechnology **20**, 015304 (2009).
[16] N. Suzuki, H. Tanaka, and T. Kawai, Adv. Mater. **20**, 909 (2008).
[17] H. S. Jung, H. Fujiwara, and S. Matsunuma, J. Magn. Magn. Mater. **286**, 229 (2005).
[18] T. Ambrose, R. L. Sommer, and C. L. Chien, Phys. Rev. B **56**, 83 (1997).
[19] M. R. Scheinfein, LLG Micromagnetics Simulator™.
[20] B. Beckmann, U. Nowak, and K. D. Usadel, Phys. Rev. Lett. **91**, 187201 (2003).